




Synthesis of Silicon Sulfide by Using CS₂ Gas



RYOSUKE O. SUZUKI , YUTA YASHIMA, TAKUMI KANEKO,
ELTEFAT AHMADI , TATSUYA KIKUCHI , TAKAFUMI WATANABE,
and GENKI NOGAMI

Silicon sulfide (SiS₂) was synthesized from Si, SiC, Si₃N₄, and a eutectic Al-Si liquid. An Ar-CS₂ gas mixture, after bubbling through liquid CS₂, was passed over pulverized Si, SiC, Si₃N₄, or a eutectic Al-Si alloy liquid. White, needle-shaped SiS₂ was precipitated as a single phase on the colder downstream surface when Si powder in a SiO₂ liner was heated over 1273 K. This deposition mechanism involves a reaction between Si and CS₂ to form SiS₂, with the vaporization of SiS(g) and deposition as SiS₂(s) from SiS(g) and S₂(g). Quartz was unaffected by the reaction gases. Notably, Si, SiC, Si₃N₄, and the eutectic Al-Si liquid were found to be suitable sources for SiS₂ synthesis, although this was suppressed owing to Al₂S₃ formation on the latter.

<https://doi.org/10.1007/s11663-021-02103-y>

© The Author(s) 2021

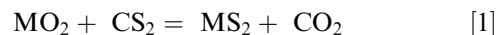
I. INTRODUCTION

METALLIC sulfides with layered morphologies, such as SiS₂, are employed in all-solid rechargeable battery electrolytes.^[1] The two-dimensional polymeric chain structure of SiS₂ makes it suitable for Li intercalation.^[2–5] Unlike some sulfides, SiS₂ is not a naturally occurring mineral and must be synthesized. This study focuses on SiS₂ synthesis from powdered Si, SiC, and Si₂N₃, as well as eutectic Al-Si liquid. The objectives of the study were as follows: (1) to determine which of the Si sources, if any, would form SiS₂; (2) to determine the reaction processing conditions for SiS₂ formation; and (3) to characterize the SiS₂ and associated products. The proposed process offers the benefit of providing a means for recycling common Si waste. This sulfide synthesis approach is applicable to catalyst formation or laterite upgrading.

The standard synthesis process for SiS₂ employs the reaction of Al₂S₃ with SiO₂ at temperatures above 1523 K.^[2–11] Direct reaction between S and Si is difficult because of the high melting point of Si, the high vapor pressure of S, and easy sublimation of SiS₂. Although some sulfides can be formed by slow heating of encapsulated metal and S powder followed by a high-temperature soak lasting weeks or months, this is too slow for commercial production. In this study, the potentially faster and lower-temperature reaction of the selected Si sources with CS₂ vapor entrained in Ar was investigated.

II. LITERATURE

Many researchers^[12–23] have investigated the reaction of metal oxides with CS₂ to form metal sulfides *via* the following reaction:



at temperatures as low as 1273 K. Even very stable rare-earth metal oxides can be converted to the corresponding sulfides or oxysulfides *via* this route.^[6] This method has been suggested for use in nuclear fuel processing, laser applications, and thermoelectric devices.^[12–25] Furthermore, CS₂ is more reducing than H₂S and has been demonstrated as a means of refining the oxides and nitrides of Ti, V, and Sc.^[26–30] Many investigators^[12–23, 26, 30–34] have used a CS₂ bubbler to produce CS₂ gas for subsequent reactions and to limit the gas circuit for safety. The selected CS₂ bath temperature was close to room temperature, between 263 K and 313 K. Previous papers published by the authors^[26, 30] reported the use of a bath at higher temperatures.

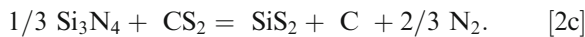
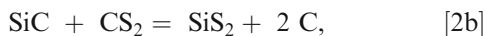
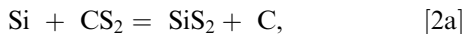
RYOSUKE O. SUZUKI and TATSUYA KIKUCHI are with the Faculty of Engineering, Hokkaido University, Kita-13, Nishi-8, Kita-ku, Sapporo, Hokkaido, 060-8628 Japan. Contact e-mail: rsuzuki@eng.hokudai.ac.jp YUTA YASHIMA is now with the Central Japan Railways Co., Minato-ku, Tokyo 108-8204 Japan. TAKUMI KANEKO is now with the Toho Titanium Co. Ltd., Yohohama, Kanagawa 220-0005 Japan. ELTEFAT AHMADI is with the Faculty of Engineering, Hokkaido University, Kita-13, Nishi-8, Kita-ku, Sapporo, Hokkaido, 060-8628 Japan and also with the Japan Society for the Promotion of Science (JSPS), 5-3-1 Kojimachi, Chiyoda-ku, Tokyo 102-0083, Japan. TAKAFUMI WATANABE and GENKI NOGAMI are with the Mitsubishi Gas Chemical Co. Inc., Chiyoda-ku, Tokyo 100-8324 Japan.

Manuscript submitted April 5, 2020; accepted January 29, 2021.

Article published online March 3, 2021.

The structure of SiS₂ is orthorhombic ($a = 0.561$ nm, $b = 0.547$ nm, $c = 0.9583$ nm^[3]), and the condensed form of SiS₂ is a white, needle-like crystal with a melting point of 1363 K.^[35–38] Notably, SiS₂ exhibits a boiling phenomenon between 1373 K and 1473 K.^[37, 39] Since its melting and boiling points are close to each other, it undergoes significant sublimation of SiS₂ below melting point.^[3, 5, 7–11, 35, 40] This phenomenon suggests that SiS₂ might be a good candidate for vapor refining; however, condensation must occur rapidly because SiS is also known to deposit from the transport gas during cooling.^[3, 4, 6–8] Any SiS₂ product must be isolated from the ambient atmosphere to prevent deliquescence and reaction with water vapor to form H₂S and SiO₂.^[4, 6–8, 40] Therefore, the product must be stored in a dry and inert atmosphere.

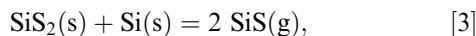
Literature published between 1880 and 1930^[6, 11, 30, 35, 41] showed that SiS₂ was formed from reactions with CS₂ in china clay reactors, indicating that Al₂O₃ and SiO₂ reacted with CS₂. However, this reaction could not be confirmed by the preliminary experiments in this study nor by the thermochemical computations^[11, 35, 36, 42, 43] described later. Therefore, SiO₂ was not selected as a Si source herein; instead, Si, SiC, Si₃N₄, and eutectic Al-Si were used. The binary Al-Si system exhibits eutectic behavior at Al-12.8 wt pct Si and at 850 K.^[44] Since Al-Si alloy is a basic Al alloy, Si recycling *via* selective sulfurization is desirable. The SiS₂ formation reactions are as follows:



Carbon contamination in SiS₂(s) does not lead to significant problems in Li battery applications.

The reaction with Al₂S₃ and SiO₂ has been used to synthesize SiS₂ since 1935.^[3, 5, 7, 9, 10, 39] Byerley and Teo reported that Al₂S₃ and SiO₂ reacted in a N₂ atmosphere at 1523 K, and that SiS₂ sublimated in vacuum at 1523 K to produce high-purity SiS₂.^[9, 10] The sublimation of SiS₂ has been reported by Haas,^[41] as well as by Schumb and Bernard,^[45] to be slow. Byerley and Teo,^[9, 10] and Emons and Theisen^[46] determined the partial pressures of sulfides and S₂ by Knudsen cell measurements, and obtained results in good agreement with others,^[42, 47] as shown in Figure 1; however, there were differences in the delineation of the pertinent reactions.

The extrapolation to 1 atm SiS(g) of the reaction



approaches the boiling point of SiS₂ (1403 K), as estimated from the JANAF tables.^[37] The boiling process of SiS₂ necessarily includes the sublimation of SiS, as written in Reaction [3].^[9, 10, 38, 46, 47] Since the early 1930s, the evaporation of sulfides has been the subject

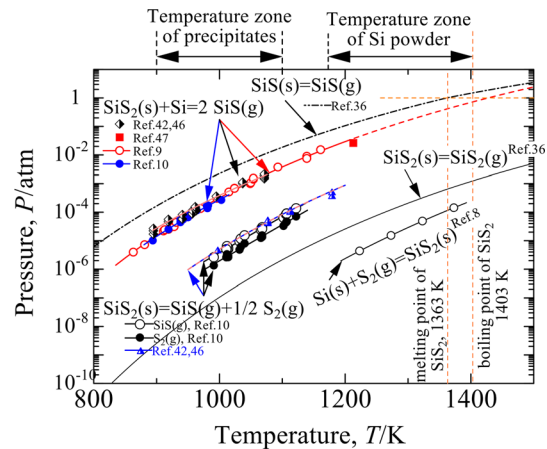
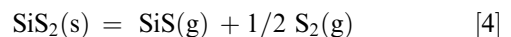


Fig. 1—Partial pressures of gases in Si-S binary system.

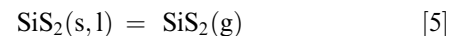
of numerous investigations,^[11, 37, 41–43] and the existence of two sulfides, namely SiS₂ and SiS, has been recognized by 1965.^[4, 10, 41]

The properties of solid SiS have not been investigated because of its strong deliquescence and subsequent disproportionation. Moreover, SiS gas has been commonly reported to form a black or gray deposits after the reactions of Si with S, H₂S, or other sulfides, such as CuS, FeS, ZnS, and Al₂S₃.^[7, 8, 10, 31, 45, 48] Additionally, SiS shows yellow, orange-red, dark brown, reddish black, and black colors because of its instability at room temperature in an ambient atmosphere.^[9, 10, 41, 45]

In 1939, Barrow and Jevons^[31] reported that SiS could be formed from Si and gaseous CS₂, although SiS and SiS₂ could not be distinguished by spectroscopic analysis of distilled SiS. Schumb and Bernard^[45] reported that SiS was formed by heating a mixture of pure SiS₂ and excess Si at 1123 K, and that SiS was not formed by the reaction between Si and S₂ gas at 1 atm. Byerley and Teo^[10] reported the decomposition of pure SiS₂(s) in the Knudsen cell to SiS(g) and S₂(g) (Figure 1). The partial pressures of the products of Reaction [4] were approximately 100 times lower than those of the products of Reaction [3].

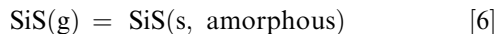


The vapor pressure compiled in HSC Chemistry^[36] for Reaction [5]



is only 6.5×10^{-4} atm at the reported boiling point of SiS₂.^[35, 37] Furthermore, the vapor pressure of SiS exceeds 1 atm at the melting point of SiS₂^[36]; therefore, SiS(g) predominates. The employed database^[36] cites JANAF thermodynamic tables,^[37] the calorimetric data^[7, 11, 43, 48] from which are favored. The contradictory reports of vapor pressure measurements have been the topic of numerous discussions^[11, 37, 41–43, 49] and the need for accurate thermochemical data persists. Herein, we use the experimental reports from the evaporation studies^[8–10, 41, 46, 47, 50] and the database summarized in HSC Chemistry,^[36] as shown in Figure 1.

Crystalline SiS has not been reported and solid SiS is formed as an amorphous structure only from condensing gaseous SiS,^[3, 9, 10, 31, 41, 45, 50] *i.e.*,



whereby SiS decomposes to Si and SiS₂ after annealing without crystallization.^[10, 33, 34, 41, 42, 45] This suggests that SiS is thermodynamically unstable and that SiS may not be formed *via* Reaction [2a].

The vaporization of SiS₂ is strongly related to the chemical reactions of the SiS system, and a possible mechanism involves the proportional reaction of Eq. [3]. The results of this approach have been shown to match that of the compositional analysis of gas mixtures by mass spectroscopy, according to Coppens *et al.*^[49]

Yokoyama³²⁾ patented the synthesis of SiS₂ by the reaction of SiC and CS₂ based on Reaction [2b]. He reported that only non-volatile carbon remained after Reaction [2b] and that SiS₂, not SiS, was evaporated. Notably, SiS₂ is condensed at the cold part of the reactor. In Yokoyama's study, 0.9 kg of SiS₂ was produced at 1073 K in 1 hour from 2.1 kg of CS₂ and 0.8 kg of SiC mixed with the clay. Such a fast reaction at relatively low temperatures is an attractive way to form SiS₂, but neither a detailed mechanism nor thermal conditions were presented, and no additional data have been reported subsequently. Therefore, the fundamental information on CS₂ gas sulfurization is the focus of this study to provide an effective means of stable synthesis of SiS₂, and perhaps, SiS.

TiO₂, TiO, TiN, and TiC have reportedly been sulfurized at 1273 K.^[15-17, 22, 26] Trivalent TiN and 4-valent TiC were sulfurized more quickly than divalent TiO.^[26, 27]

Industrial quantities of CS₂ liquid are available for commercial processing and thermochemical data are available for CS₂ gas sulfurization; thus, it is possible to analyze the chemical processes involved in SiS₂ synthesis.

III. THERMOCHEMICAL

Figure 2 shows the standard Gibbs free energy changes (ΔG°) for the reactions to form SiS₂ from Si, SiC, and Si₃N₄.^[36] Since they are negative at all temperatures, the reactions from Si, SiC, and Si₃N₄ are favorable when the reactants are in their standard states, which are the pure condensed phases and ideal gases at unit activity.

The binary Al-Si system shows a simple eutectic melting behavior at Al-12.8 wt pct Si and 850 K.^[44] The dilution of Si as the mixture reduces the thermochemical activity of Si, and a slight negative deviation from the ideal mixing behavior is known in Al-Si binary system.^[44, 51] Although the modification due to less activity depends on temperature and Si concentration, it consequently increases ΔG from ΔG° for Reaction [2a] shown in Figure 2. At 1473 K and the eutectic composition, for

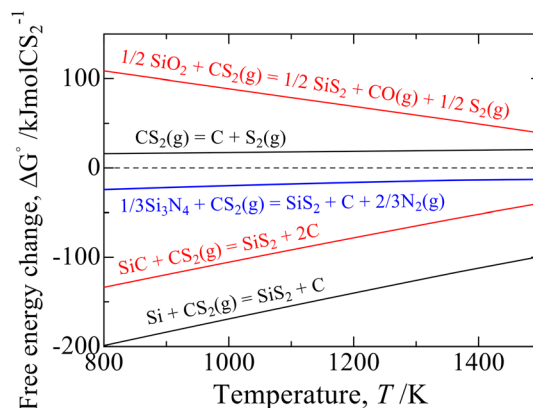
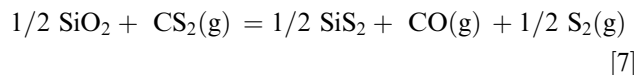


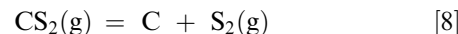
Fig. 2—Standard Gibbs free energy changes involved in CS₂ gas sulfurization.

example, the activity of Si relative to pure solid Si is 0.067,^[44] and ΔG for Reaction [2a] increases from ΔG° by +33 kJ, although ΔG is sufficiently negative to drive Reaction [2a].

Reaction [7] from SiO₂ is significantly positive at all temperatures, confirming that SiO₂ is unreactive, thereby making it suitable for reactor construction.



The positive deviation is much greater if CO₂ is the C-bearing product. In this study, SiO₂ was used as a non-reactive material in CS₂ gas flow. The thermal decomposition of CS₂ gas *via* high-temperature reaction, *i.e.*,



is also insignificant if partial pressures of both CS₂ and S₂ are near 1 atm. However, the positive value of ΔG° is not large enough to completely obviate the partial decomposition of CS₂; thus, it should be considered.

The thermal decomposition of CS₂ *via* Reaction [8] occurs partially. The Gibbs free energy change for Reaction [8] is +19.1 kJ/mol at 1273 K^[36] for the reference states of pure graphite and gases with unit activity, giving an equilibrium constant of 0.167. This means that the S₂ pressure will be 16.7 pct of the CS₂ pressure under the reasonable assumption of ideal gas behavior. A typical CS₂ partial pressure in the Ar feed stream is evaluated as the equilibrium vapor pressure at the CS₂ bath temperature. Figure 3 shows the vapor pressures of CS₂ at the bath temperature and the reaction temperature, *i.e.*, $P_{\text{CS}_2}(T_{\text{bath}})$ and $P_{\text{CS}_2}(T)$, respectively. The figure also shows the partial pressure of S₂, $P_{\text{S}_2}(T)$, at the reaction temperature T , *via* the thermal decomposition of CS₂ when carbon is at unit activity and the Ar pressure is the same at both temperatures. For example, the partial pressure of S₂ at 1273 K is as high as 0.028 atm, corresponding to $P_{\text{CS}_2} = 0.196$ atm at 273 K.

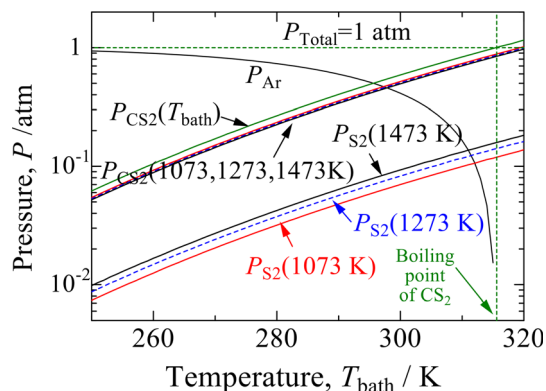


Fig. 3—Partial pressures of Ar, CS₂, and S₂ gases at temperatures of evaporation and reaction.

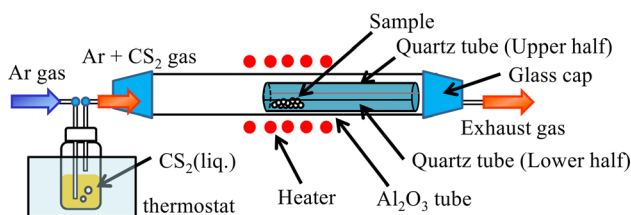


Fig. 4—Experimental setup for the sulfurization process.

The various possible reactions in the C–S–Si system complicate the sorting out process of the significant reactions from the insignificant ones. Herein, the reactions involved in the experiments are analyzed from a thermodynamic perspective.

IV. EXPERIMENTAL

Single-crystal semiconductor-grade lump Si (>99.9999 pct) was ground and sieved into -100 mesh powder. Powdered SiC (>99 pct) and Si₃N₄ (>99 pct) were obtained from Kojundo Chemical Lab. Co., Ltd. Their particle sizes were as large as 2–3 μm. The Al-12.6 wt pct Si eutectic was alloyed in air using pure Al (99.995 pct) from Nippon Light Metals Co. Ltd and an Al-25 wt pct Si alloy from Hirano Seizaemon Syouten Co. Ltd. The cast ingot was cut into small pieces after the oxidized surface was removed. Liquid CS₂ (>99.5 pct) was obtained from Fujifilm Wako Pure Chemical Corp.

Figure 4 shows the experimental setup. Pure Ar gas (>99.9998 pct) was bubbled at a constant rate into a bottle containing 50 mL of liquid CS₂ kept in a water bath at a constant temperature (± 0.2 K). The CS₂ vapor pressure generated an adequate Ar-CS₂ gas mixture.^[36] The CS₂ mass was recorded as sulfurization proceeded; it was found to vary linearly with time^[26, 27, 30] and was found to be sufficient for the sulfurization of 0.5 g Si over 1 hour. The CS₂ feed rate was controlled by a constant flow of Ar and by varying the CS₂ temperature. The linear decrease in mass with reaction time

indicated that the bubbler produced a Ar-CS₂ gas mixture of constant composition and that adequate heat was being supplied to the liquid to satisfy the enthalpy of CS₂ liquid vaporization.

A typical CS₂ feed rate at 273 K was 11.5 mL/min (8.6 x 10⁻⁶ mol/s), which was achieved with an Ar flow rate of 10 mL/min. The CS₂ bath temperature was selected to be either 273 K or 283 K.

A 40-mm-ID 1-m-long dense alumina (>99.5 pct) tube was set in the 0.5-m-long electric furnace. The unreacted exhaust gas was captured in a 1.0 M NaOH solution.^[26, 27, 30, 33, 34, 39, 48, 52] Alternatively, CS₂ could have been recovered by using a gas chiller. The temperature of the sample was monitored and controlled at the external surface of the alumina tube. The temperature profile inside the alumina tube was measured precisely in a stream of Ar gas before the sulfurization process, such that the sample temperature in the hot zone was accurately known.

Samples were held in an Al₂O₃ (>99.95 pct) boat (14 mm wide, 100 mm long) for runs 1–4 and 13–15 or in a transparent 16-mm-ID quartz tube that was 100, 150, or 300 mm long for runs 5–10. The samples for runs 5–10 were placed upstream, in the hot region of the quartz tube. The cold end of the tube was downstream and was maintained at a controlled temperature, as shown in Figure 4. The 150-mm-long tube consisted of two pieces, the upper and lower halves, to easily retrieve the condensates. The quartz tube with the sample powder was evacuated and then heated in Ar gas. The gas mixture of Ar and CS₂ was then introduced after reaching the desired temperature. Both heating and cooling were conducted under pure Ar flow at a constant flow rate (20 mL/min). The sample mass was recorded after cooling to quantify the sulfurization degree.

The resulting phases were identified by X-ray diffraction (XRD) analysis using Philips X’Pert Pro (Cu K α). The morphology of the specimens was determined by using a JEOL JSM 6510LA scanning electron microscope (SEM) equipped with an energy-dispersive X-ray spectrometer (EDS). The C and S concentrations were determined *via* infrared spectroscopy analysis using LECO CS-600 and oxygen concentration was measured by the inert-gas fusion method using a LECO TC-600 analyzer.

After the initial Si run series with Si, all subsequent runs employed a transparent quartz tube inserted inside the Al₂O₃ tube, as shown in Figure 4, to prevent possible reactions with Al₂O₃.

When the samples were cooled to room temperature after each run and were still in Ar atmosphere, both ends of the quartz tube were sealed with the rubber caps and placed in a glovebox filled with dry, oxygen-free Ar gas. The tube consisted of three 100-mm-long pieces to facilitate precipitate recovery. The Si source was placed at the hot end of the tube, such that it was positioned in the hottest zone in the alumina tube. The liquid CS₂ was typically maintained at 293 K under a constant Ar flow rate of 10 mL/min.

Table I. Experimental Condition for Sulfurization of Si Powder

Run	CS ₂ Temp. (K)	Sample Temp. (K)	Time (hours)	Ar Gas flow rate (mL/min)
1	273	873	4	20
2	273	973	4	20
3	273	1073	4	20
4	273	1173	4	20
5	273	1473	20	20
6	273	1473	4	20
7	273	1273	8	20
8	273	1273	4	20
8N*	NA	1273	4	20
9	283	1273	4	20
10	273	1273	2	20
13	283	1473	20	10
14	283	1273	16	20

*The initial sample was SiS₂ powder.

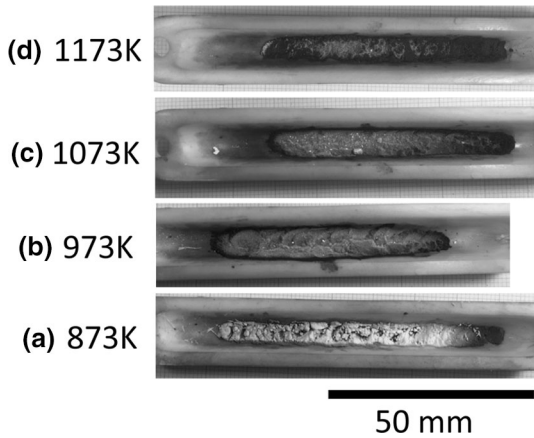


Fig. 5—Appearance of the samples (runs 1-4) in the alumina boats after sulfurization for 4 hours at various temperatures.

V. RESULTS

The results from reacting CS₂ to sulfurize Si, SiC, Al-Si eutectic alloy, and Si₃N₄ are presented for each Si source.

A. Sulfurization of Si powder

The sulfurization of Si was initially performed in an Al₂O₃ boat and then in a SiO₂ liner to avoid potential reactions with Al₂O₃. The experimental conditions are listed in Table I.

1. Synthesis in Al₂O₃

White powder, identified as SiO₂, was found to lightly coat the Si particles as the conclusion of run 1, as shown in Figure 5(a). This was probably the result of the unintentional moist air hydrolysis of SiS₂ or SiS.^[7, 11, 33-35, 41, 45] A thin glossy gray layer, similar to tar, was found adhered to the alumina boat after runs 2-4. The XRD patterns showed this to be primarily α -Al₂O₃, possibly with some amorphous SiS.^[9, 10, 41, 45] Most of the residue remained as unreacted Si, even after 4 h. Single-phase SiS₂ could not be synthesized at the initial position of the Si powder in the Al₂O₃ boat. Several thermochemical reactions occur between Si and CS₂ gas.

Significant amounts of white, needle-like SiS₂ precipitates were found in the lower-temperature region of the Al₂O₃ tube. The size of this precipitation became more longer and the larger amount of precipitates were found as the Si powder was heated to higher temperatures.

2. Synthesis in SiO₂

Figure 6 shows a black product, which remained only near the hot end, while the white, needle-like precipitates were formed 100 mm from the furnace center, where the temperature was ~900 K. This result agrees with those of

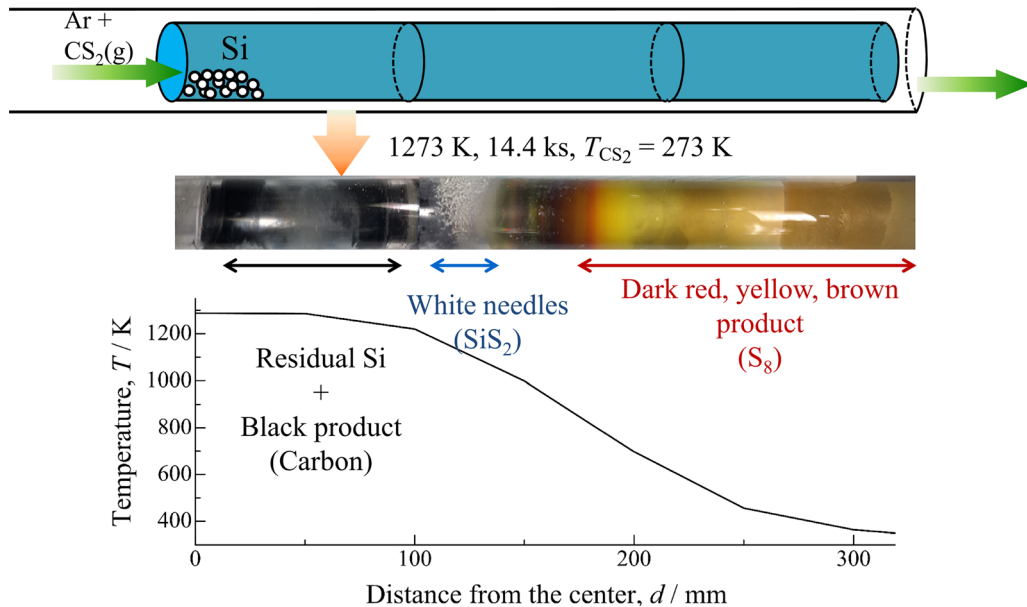


Fig. 6—Appearance of SiO₂ tube after sulfurization; temperature profile and the precipitates in the tube, where the Si powder was heated at 1273 K for 4 hours (run 8).

runs 1–4 that make use of an Al_2O_3 boat. Farther downstream, dark red precipitates were gradually transitioned to yellow.

No precipitates were found in the few millimeter-long gap between the inner SiO_2 and the outer Al_2O_3 tubes. Furthermore, no product was precipitated upstream from the initial sample position, meaning that the flow of reaction gas carried or generated the condensate downstream. The white needles or sometimes thin and long plates grew in the upstream and inward radial directions, as shown in Figure 7.

Using the upper- and lower-half tubes of silica, the quantity of the white product on the inner surface of the half tubes was recorded for several runs. The amounts were identical in both halves, and the precipitates had similar morphologies. Gravity had no discernable effect and no trace of liquid was found after runs 7 and 10. Therefore, the white precipitates were deposited from the gas onto the cold substrate and were not hydrolyzed.

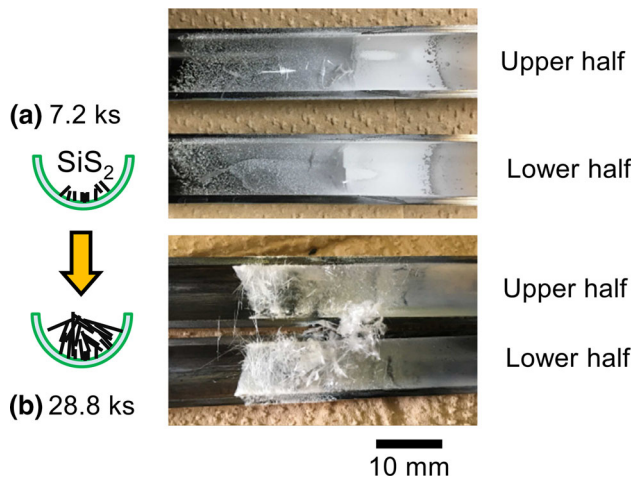


Fig. 7—White precipitates on the inner surface of SiO_2 half tubes from (a) run 10 (1273 K, 2 hours) and (b) run 7 (1273 K, 8 hours).

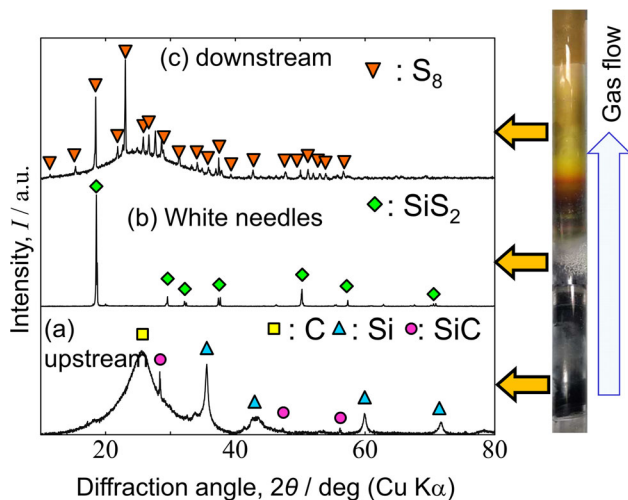


Fig. 8—XRD patterns of the specimens taken from the various parts of the tube in run 8.

Figure 8 shows the XRD spectra for selected sample locations for run 8 (1273 K, 4 hours). Notably, SiS_2 was absent at location (a), the initial position where the Si powder was placed. Near the center of the quartz tube, at location (b), the white deposit was identified as SiS_2 . Most of the initial Si powder was converted to an amorphous phase, while a lesser amount was transformed to SiC . The small amount of the black or gray material between the initial Si position and the position of SiS_2 deposition could not be identified through XRD analysis. This material was very thin and highly hygroscopic, thereby suggesting that it was an amorphous SiS precipitate. The yellow deposit downstream from SiS_2 deposition was identified as S_8 , which is the stable form of solid sulfur. The broad halo pattern in XRD indicated the existence of either amorphous S or amorphous SiS . Notably, S exhibits a yellow or brownish color when it solidifies from liquid, depending on its purity and thickness.

Figure 9 shows the elemental analysis of the white precipitates produced in 2 hours at 1273 K using an Ar- CS_2 mixture generated at 273 K. The sample prepared in run 10 was identified as SiS_2 by XRD analysis; however, more than 4 hours at 1273 K was necessary to determine the Si/S ratio of the phases.

B. Sulfurization of SiC

Fine SiC powders ($2\text{--}3\ \mu\text{m}$) were heated to 873 K for 3 days and to 1073 K for 1.5 day. Thereafter, Ar gas was bubbled at a rate of 10 mL/min through liquid CS_2 at 293 K. The color, size, and XRD patterns of these samples were those of pure SiC and unchanged, as shown in Figures 10(b) and (c). There were no deposits in the furnace even after a very long reaction time at these low temperatures.

SiC powder was exposed to the mixed gas at 1273 K for 1 day. The appearance of the tube was identical with that when pure Si was used. Needle-shaped crystals of SiS_2 precipitated downstream on the quartz wall. The position of deposition, as well as the XRD spectra, was also identical as with the use of Si powder (Figure 10(e)).

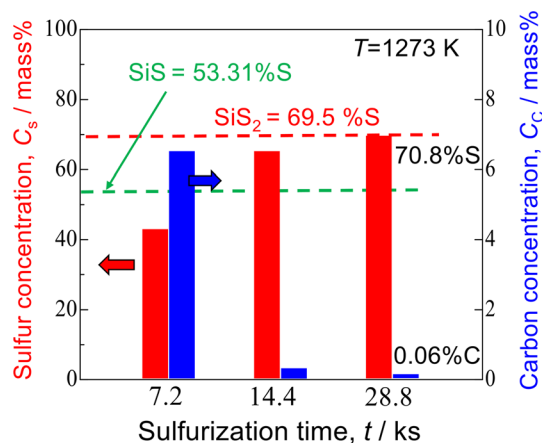


Fig. 9—Elemental analysis of sulfur and carbon in the white precipitates obtained at 1273 K.

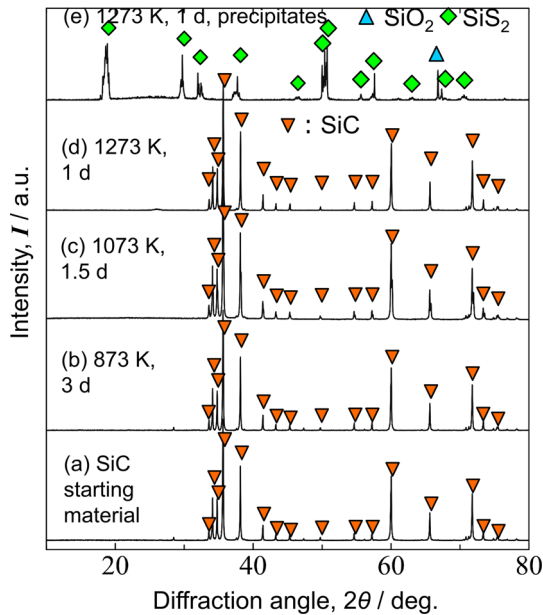


Fig. 10—XRD patterns of SiC powder after heating in Ar-CS₂ gas mixture at various temperatures.

C. Sulfurization of liquid Al–Si eutectic

Two 3.5-g samples of Al-13 wt pct Si alloy were, in separate runs, set in an Al₂O₃ boat and reacted for 1 day in a mixture formed by bubbling 10 mL/min of Ar through liquid CS₂ at 293 K. The Al–Si alloy was not stirred. One sample was heated to 873 K and the other to 1273 K. Both had solidified surfaces after cooling, indicating melting.

At 873 K, no deposition of needle-shaped crystals was found in the colder regions of the furnace. The sample heated at 1273 K, however, formed needle-shaped crystals downstream. The XRD results shown in Figure 11 confirmed the presence of single-phase SiS₂ without Al contamination. However, the metallic luster of the Al–Si alloy was lost and sulfurized to black after solidification at 1273 K. Notably, the product on the alloy surface was identified to be α-Al₂S₃ via XRD analysis.

D. Sulfurization of Si₃N₄

Figure 12 shows the result when the same Ar-CS₂ gas mixture was generated by bubbling 10 mL/min Ar through CS₂ liquid at 293 K, after passing over the Si₃N₄ powder in the transparent quartz at 1273 K for 1 day. White, needle-shaped crystals precipitated on both the upper and lower halves of the tube in the cold region. These were identified by XRD as single-phase SiS₂. The Si₃N₄ powder was placed more widely than the previous samples, but only the powder at the hottest region changed its color, as shown in Figure 12. The region between the hottest area of Si₃N₄ and the SiS₂ deposition area was slightly covered with black particles, which could not be identified by XRD because of their small mass and reactivity. The black–gray particles were found only at the lower half of the tube.

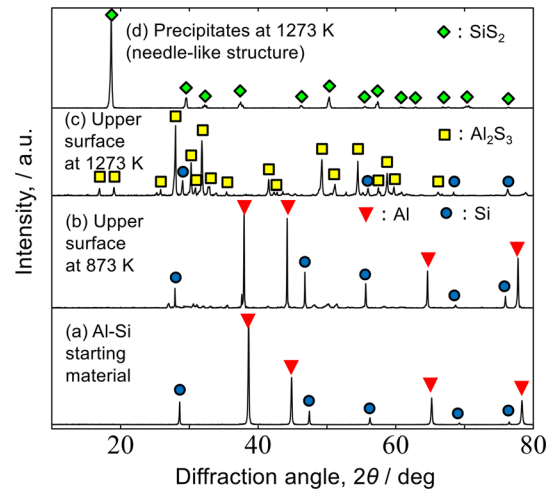


Fig. 11—XRD patterns of Al–Si alloys, where the reaction time was set commonly to 1 day.

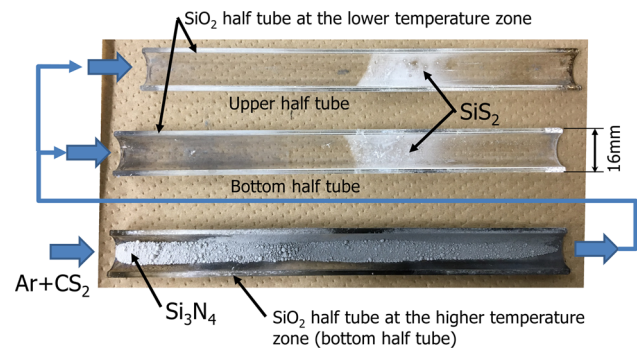


Fig. 12—Appearance of sulfurized sample and white precipitates on the inner surface of SiO₂ tube.

Figure 13 shows the XRD patterns of the samples heated for 1 day at temperatures lower than 1273 K. There were neither precipitates of SiS₂ crystals nor phase change of Si₃N₄ at 873 K, 973 K, and 1073 K observed. When the sample was heated to 1173 K, a small amount of SiS₂ precipitates, as shown in Figure 13(f), was observed. Furthermore, SiS₂ crystals were formed at the lowest temperature (1173 K) among the four materials studied when Si₃N₄ was used.

VI. DISCUSSION

A. Sulfurization of Si powder

1. In Al₂O₃

The expected direct Reaction [2a] did not occur in runs 1–4 at the hottest regions in the furnace. Reaction [9] at the hot zone was expected to form amorphous carbon and gaseous SiS, followed by its partial deposition as amorphous SiS, as shown in Reaction [10].

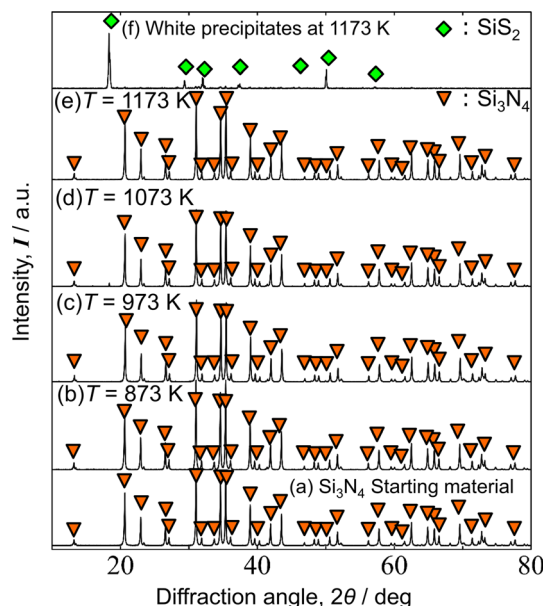
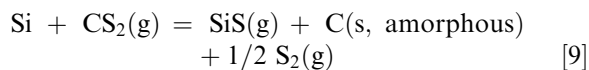
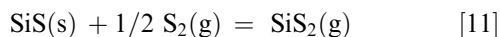


Fig. 13—XRD patterns of Si_3N_4 samples, where reaction time was set commonly to 1 day and liquid CS_2 was kept at 293 K under Ar flow rate of 10 mL/min. (a): starting material, Si_3N_4 , (b) through (e): after sulfurization at 873 K, 973 K, 1073 K, and 1173 K, respectively, (f) white powder precipitated by sulfurization at 1173 K.



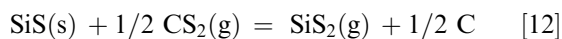
The formation of $\text{SiS}(\text{g})$ may preferentially occur through Reaction [9] at the high-temperature zone. The vaporized $\text{SiS}(\text{g})$ may then be carried by the gas flow to decompose and condense as SiS at the lower-temperature zone^[10, 46] via Reaction [10]. The formation of crystalline SiS was neither reported in the literature nor detected in this work.

Gaseous SiS may decompose to $\text{SiS}_2(\text{s})$ and $\text{Si}(\text{s})$ as the reverse of Reaction [4]. However, the co-deposition of $\text{Si}(\text{s})$ with $\text{SiS}_2(\text{s})$ was not detected. A possible route to form $\text{SiS}_2(\text{s})$ from the gas phase remained only in Reaction [11], i.e., a route via $\text{SiS}(\text{g})$.



SiS once deposited is transformed to SiS_2 by exposed to $\text{S}_2(\text{g})$, and it again evaporates as $\text{SiS}_2(\text{g})$. The black or gray deposition with a strong hygroscopic property in addition to the odor of H_2S upon exposure to air can be tentatively identified as amorphous SiS . The coexistence of $\text{S}_2(\text{g})$ is key to SiS_2 crystals by Reaction [11] because the parallel evaporation Reaction [3] does not form the $\text{S}_2(\text{g})$ required by Reaction [11].

Another possible reaction for $\text{SiS}(\text{g})$ deposition is that with $\text{CS}_2(\text{g})$ as:



Nevertheless, carbon deposition was not observed; thus, Reaction [12] was dismissed as a viable path to produce SiS_2 . Although SiS_2 vaporization was independently observed in this work, its pressure was thermodynamically 1000 times lower than that of SiS vaporization, as shown in Figure 1.

2. In SiO_2

The needle-like samples shown in Figure 14(a) were analyzed by elemental mapping. They exhibited a homogeneous distribution of O, Si, and S. The trace amounts of C were probably from the carbon tape used for SEM sample preparation. Carbon was not detected in the crystalline grains. The O profile showed that the crystal surface contained a considerable amount of oxygen, which was expected as the specimens were heavily oxidized. However, this does not correspond to the XRD data that show the SiS_2 phase. The XRD profiles of this specimen were first measured in air and again after keeping in vacuum for 5 days, where EDS mapping revealed that a SiS_2 phase had transformed into a mixture of crystalline and amorphous phases, probably SiO_2 . Because of the extreme sensitivity to hydrolysis, the surface may have decomposed into a very thin and amorphous SiO_2 layer during handling. The characteristic H_2S smell effusing from the sample supported the hydrolyzation hypothesis. The intensity of S, as shown in Figure 14(c), seems very low because of its low-intensity energy profile and the overlapping profiles with the other elements. The detected signal positions of S agreed with the locations of Si. Therefore, neither free C nor free S from the CS_2 gas is attached to the SiS_2 surface. This is consistent with the element analysis shown in Figure 9.

The specimens were slightly oxidized during the transfer for analysis, and the precipitate volume was very small for short-time sulfurization, thereby preventing the separation of the needle-shaped SiS_2 crystals from the surrounding tar-like amorphous material adhering as a thin sheet to the silica tube. As shown in Figure 9, a highly purified SiS_2 was recovered from the central part of the tube at a longer sulfurization time. A small amount of carbon in the samples may have been present because of the sampling method. This phenomenon is consistent with SiS_2 vapor deposition. The morphology and microstructure of the precipitated SiS_2 samples are shown in Figure 14. The white precipitates resembled needles in macroscopic view, although they were assemblies of long square pillars. This directional growth is consistent with the orthorhombic SiS_2 structure.

B. Sublimation of SiS

The vapor transport behavior of SiS_2 was studied in the absence of CS_2 by placing 1 g of SiS_2 in the hot end of the SiO_2 tube to observe its transport to the colder regions of the reactor. The vapor pressures of the solid SiS_2 , defined according to equation,^[5] are 1.22×10^{-4} and 1.05×10^{-7} atm at 1273 K and 1000 K, respectively, while $\Delta H_{\text{subl}}^{\circ}$ is 273.2 kJ/mol.^[36] The sample was held at 1273 K for 4 hours in run 8N while pure Ar gas,

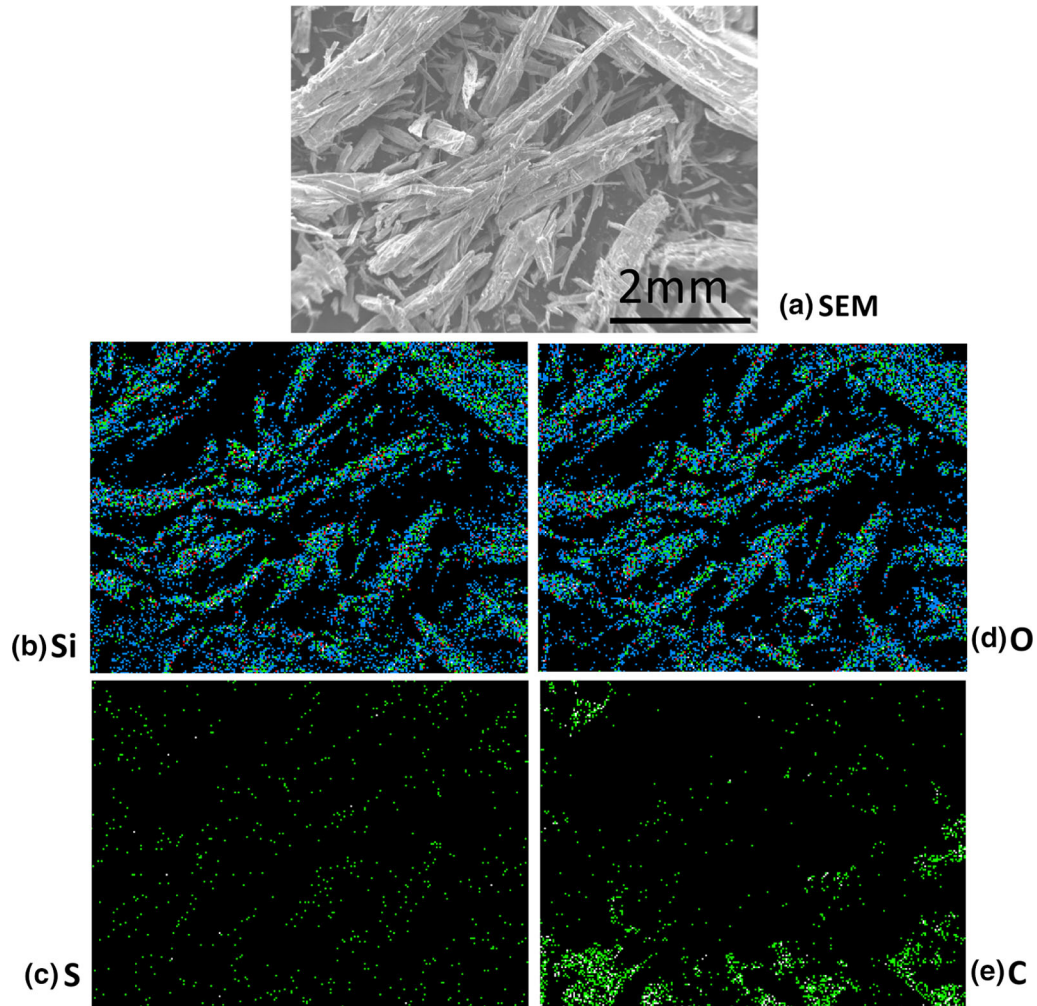


Fig. 14—SEM image (a) and its element mapping of (b) silicon, (c) sulfur, (d) oxygen, and (e) carbon, of the specimen at run 8.

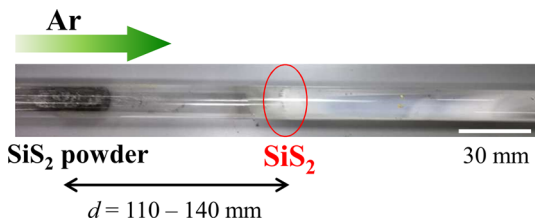


Fig. 15—Photo of the quartz tube after heating SiS_2 in an Ar atmosphere at 1273 K (run 8N).

devoid of CS_2 , was passed through the furnace at a 20 mL/min flow rate. The linear velocity of the Ar flow was as minimal as 1.15×10^{-3} m/s.

Figure 15 shows a photograph of the cooled quartz tubes after the heating cycle. White, needle-shaped SiS_2 crystals were deposited downstream. The deposition position was approximately 110 to 140 mm from the initial position of SiS_2 , which corresponded to 1023 K to 1173 K based on the profile shown in Figure 6. This is approximately 100 degrees higher than the deposition of SiS_2 derived from the reaction of CS_2 with the selected Si

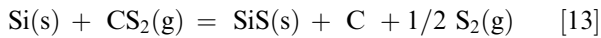
sources. This 100 K higher SiS_2 condensation temperature indicated that the vapor pressure of the evaporation-derived SiS_2 was less than those obtained from the CS_2 reactions.

A small quantity of white precipitate was also found on the lower half of the upstream tube, and it was symmetrical with the downstream deposit. This symmetry indicated that SiS_2 diffusion was fast compared to bulk flow. This upstream deposition was not observed in Ar- CS_2 sulfuration. The sublimation-generated SiS_2 is thought to have caused accelerated back diffusion and upstream deposition, whereas CS_2 -derived deposition ensues downstream deposition only. Furthermore, the orange-black deposits are unrelated to SiS_2 vapor transport but associated with reactions involving CS_2 . The mechanisms of evaporation and deposition are different in these two cases.

These observations show that although SiS_2 vapor transport occurs without CS_2 , the reaction of CS_2 with Si sources will generate SiS_2 at a rate that is three orders of magnitude slower than the SiS_2 vaporization rate.

C. Reaction Mechanism

Figure 16 shows a suggested reaction path schematic. The CS₂ gas evaporates from the liquid into the Ar carrier gas at approximately room temperature. This gas passes into the high-temperature region and reacts with Si. Because neither SiS(s) nor SiS₂(s) was observed on the Si surface, their precipitations were neglected by combining Eqs. [6] and [9] to give:



The resulting C was observed to be amorphous. The C is proposed to react with Si to generate SiC, although the reaction is believed to be slow.



Carbon contamination in SiS₂(s) does not cause significant problems in Li battery applications.

This reaction sequence exhausts S₂(g), as shown in column 1 of Figure 16. The second column shows that a simultaneous reaction between Si and CS₂ gas generates SiS(g) followed by subsequent condensation in the colder regions of the reactor. The formation of SiS₂(s) on the Si surface and its vaporization as SiS(g) are feasible as the side reaction, as shown in the third column. The far-right path shows the condensation of S₈ due to cooling from the S₂(g) originating from the thermal decomposition of CS₂, as well as the decomposition of SiS₂ to SiS.

Figure 17 presents an illustration of the gas pressures at the vaporization^[9] and the successive deposition^[4] from Si + CS₂, referring to Figure 1. These two reactions (upper and middle lines in Figure 17) are irreversible under gas flow. The evaporated SiS(g) at T₂, as shown by the upper curve (red), is condensed as SiS₂(s) by reacting with S₂(g), as shown by the middle curve (black). A large amount of SiS(g) at 1273 K, for example, is carried to the

lower-temperature area, whereas SiS(g) decomposes and condenses to solid SiS₂ (middle curve). Based on the measurements of equilibrium vapor pressure among SiS₂, SiS, and S₂,^[10, 41, 46] as shown in Figure 1, once SiS(s) is formed, it cannot exist at the higher temperature area because of the high vapor pressure of SiS(s). Under the exposure of S₂(g) and by absorbing S₂(g), SiS(g) deposits as SiS₂(s). When this pressure is estimated to be as high as 10⁻⁶ atm, the temperature is evaluated as 951 K. Without the coexistence of S₂(g), the pressure of SiS₂(g) is low, as reported by Rosenqvist and Tungsavik.^[8] The vaporization of pure SiS₂(s) was independently examined and the deposit was found at 1073 K. (lower dashed curve in Figure 17). Therefore, the deposition temperature from SiS₂(g) is 122 K different from the former mechanism *via* SiS(g).

Figure 1 quantitatively shows the vapor pressure of solid SiS₂ by Reaction [5].^[36] Its vapor pressure ranges from 3.5 × 10⁻³ atm at 1473 K to 1.4 × 10⁻⁵ atm at 1173 K. Vapor transport rate in an Ar carrier gas is directly related to the product of the partial pressure of the transport species and the Ar flow rate. The low transport rate from SiS₂(s) also agrees with the relatively low pressure of SiS₂ in the Ar carrier gas.

The vapor pressures of SiS and S₂ are higher than that of SiS₂, as shown in Figure 1 if pure solid SiS₂ exists at a constant temperature. This indicates the preferential evaporation as SiS(g) and S₂(g). The sharp temperature dependencies of the reactions related to SiS(g) suggest that the deposition from SiS(g) as SiS₂(s) preferentially occurs in the lower-temperature regions.

D. Sulfurization of SiC

After the runs for SiC, SiS₂ precipitated at 1273 K. However, a significant fraction of the SiC powder remained unreacted at 1273 K, contrary to a patent claiming good recovery at 1073 K for 1 hour.^[32] In the runs for Si, a small amount of SiC is one of the intermediates from Si to SiS₂ as SiC is converted into SiS₂ by the additional sulfurization under the same gas flow conditions.

The deposition position was also identical as obtained with the use of Si powder, the same as the XRD spectra (Figure 10(e)). The formation of SiS₂ from SiC is favorable, but a minimum temperature of 1273 K is required for the SiC starting material.

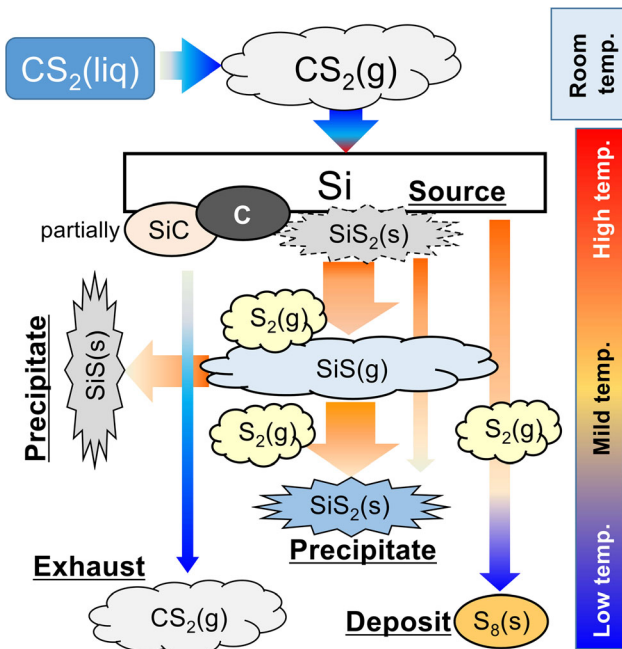


Fig. 16—A schematic of sulfurization mechanism when Ar/CS₂ gas was used.

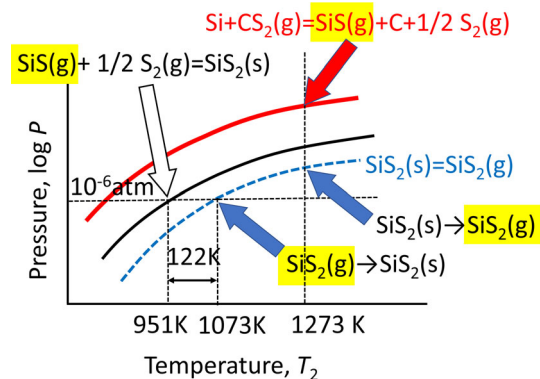


Fig. 17—Temperature dependencies of pressures related to the reactions.

1. Potential Diagram

Carbon deposits on the unreacted Si particles *via* Reaction [9]. This may produce SiC, as shown in Figure 16. However, SiC can form SiS₂, as shown in Figure 10. Therefore, the total stability of the Si–S–C ternary system should be considered. Both the reactivity between the Si and CS₂ gas, as well as that between the SiC and CS₂ gas, can be summarized by the potential diagram shown in Figure 18, which is based on the employed database.^[36] Although the thermodynamic database may need refinement, it provides a potential diagram that approximates the phase stability at 1273 K. The standard state activity of C, a_C , is pure solid graphite, which is very similar to the activity of amorphous C deposits. Additionally, the S pressure cannot exceed 1 atm because the system is constrained to remain at atmospheric pressure by the bubblers. Similarly, the partial pressure of the CS₂ gas depends on the bath temperature, T_1 , which is also less than 1 atm.

The potential diagram shown in Figure 18 was constructed based on the following conditions: The cross-hatched region is the feasible operating area to produce the reactive Ar-CS₂ gas mixture; An equilibrium point lies in this region, especially on the line of $a_C = 1$ in the stable SiS₂ region if stable graphite coexists. Activities of C less than unity represent that the gas is not saturated with C; thus, the locations where $a_C < 1$ denote conditions of no carbon deposition and the region where $a_C > 1$ indicates the possible existence of amorphous C.

The region of solid SiS only exists at $a_C \ll 1$; thus, it cannot exist in the presence of pure C. High partial pressure of S₂ is beneficial for CS₂ gas sulfurization, and such a condition is envisaged from the thermal decomposition of CS₂. The red line of 2.56×10^{-4} atm S₂ pressure was computed from the liquid CS₂ being at only 200 K. The residual C from the decomposed CS₂ gas did not contaminate the SiS₂ product owing to the SiC coexistence. Higher S₂ partial pressure conditions favor SiS₂ formation as a single-phase without SiC contamination.

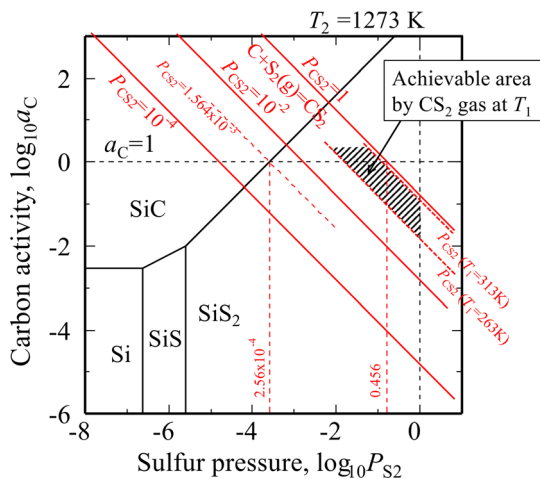


Fig. 18—Potential diagram of Si–S–C system at 1273 K and equilibrium pressures of CS₂ gas evaporated at T_1 .

E. Sulfurization of liquid Al–Si eutectic

Because the melting point of Al₂S₃ was 1373 K,^[36] the lighter and unsublimated solid Al₂S₃ floated on the surface of the liquid alloy. The Al₂O₃ crucible was unaffected by the environment, but the metallic Al alloy was readily converted into Al₂S₃ at 1273 K. The SiO₂ crucible was not used in this experiment to avoid the confusion on the reaction between Al₂S₃ and SiO₂.^[9, 10]

The formation of Al₂S₃ consumes CS₂ gas, and the covering of the liquid surface by Al₂S₃ may slow down the gas reaction between the Al–Si melt and CS₂. However, quantitative analyses, such as phase equilibrium^[39] and reaction kinetics, were not conducted because of the hygroscopic nature of SiS₂.

F. Sulfurization of Si₃N₄

Notably, Si₃N₄ reacted with CS₂ to form SiS₂, whereas SiO₂ did not. The formation of heavy gas, such as SiS, is presumed to be the cause of the formation of the black–gray particles found at the lower half of the SiO₂ tube.

VII. CONCLUSION

In this study, SiS₂ was vapor-deposited using transparent silica tubes when Si, SiC, Si₃N₄, or Al–Si eutectic alloy was heated in a mixture of Ar and CS₂(g) above 1273 K. Notably, SiS₂ was also formed at 1173 K from Si₃N₄. The needle-shaped SiS₂ crystals were precipitated at the downstream of gas flow at temperatures between 1073 K and 1173 K. They were semi-transparently white with minimal C contamination, as well as exhibited strong hygroscopic reactions in the open air and were easily oxidized to SiO₂.

Consequently, a reaction mechanism is proposed consisting of the following: (1) evaporation of SiS after the reaction between Si and CS₂, which is triggered by SiS₂(s) formation and (2) successive deposition of SiS₂(s) from SiS(g) at the low-temperature zone. The vaporization of the S₂(g) by-product plays an important role in the deposition of SiS(g) as SiS₂(s). A small amount of C contaminated the sample at the early stage proposed because of the thermal decomposition of the CS₂ gas. At the later stage, C was removed by the excess amount of S₂(g). A highly pure SiS₂(s) can be obtained at 1273 K from low-quality Si sources using high partial pressure of S in CS₂ gas.

ACKNOWLEDGMENTS

The authors thank the technical supports of SEM observation by Mr. N. Miyazaki. A part of this work was conducted at Laboratory of XPS analysis, Joint-use facilities, Hokkaido University, and supported by “Nanotechnology Platform” Program of the Ministry of Education, Culture, Sports, Science and Technology (MEXT), Japan. This work was also financially sup-

ported by Grant-in-Aid from MEXT (KAKENHI) under contacts Nr. 17H0343409 and 18F1805409 and from Japan Mining Industries Association. One of the authors (E.A.) acknowledges a fellowship from JSPS postdoctoral program (P18054).

OPEN ACCESS

This article is licensed under a Creative Commons Attribution 4.0 International License, which permits use, sharing, adaptation, distribution and reproduction in any medium or format, as long as you give appropriate credit to the original author(s) and the source, provide a link to the Creative Commons licence, and indicate if changes were made. The images or other third party material in this article are included in the article's Creative Commons licence, unless indicated otherwise in a credit line to the material. If material is not included in the article's Creative Commons licence and your intended use is not permitted by statutory regulation or exceeds the permitted use, you will need to obtain permission directly from the copyright holder. To view a copy of this licence, visit <http://creativecommons.org/licenses/by/4.0/>.

REFERENCES

1. M. Murayama, R. Kanno, M. Irie, S. Ito, T. Hata, N. Sonoyama, and Y. Kawamoto: *J. Sol. Stat. Chem.*, 2002, vol. 168(1), pp. 140–48. <https://doi.org/10.1006/jssc.2002.9701>.
2. W. Büssen, H. Fisher, and E. Gruner: *Naturwissenschaften*, 1935, vol. 23, p. 740. <https://doi.org/10.1007/BF01498156>.
3. E. Zintl and K. Loosen: *Z. Phys. Chem. (Leipzig) A*, 1935, vol. 174(3), pp. 301–11.
4. C.T. Prewitt and H.S. Young: *Science*, 1965, vol. 149(3683), pp. 535–37. <https://doi.org/10.1126/science.149.3683.535>.
5. J. Peters and B. Krebs: *Acta Crystallogr. B Struct. Crystallogr. Cryst. Chem.*, 1982, vol. B38, pp. 1270–72. <https://doi.org/10.1107/S0567740882005469>.
6. J.W. Mellor: *Comprehensive Treatise on Inorganic and Theoretical Chemistry*, vol. VI, C (Part II), §60. Si, Silicides, Longmans, Green and Co. Ltd., London, 1930, pp. 985–90.
7. P. Rocquet and M.F. Ancey-Moret: *Mémoires Présentés à la Société Chimique*, 1954, vol. 7, pp. 1038–43.
8. T. Rosenqvist and K. Tunesvik: *Trans. Faraday Soc.*, 1971, vol. 67, pp. 2945–51. <https://doi.org/10.1039/TF9716702945>.
9. J. Byerley and W.K. Teo: *Mater. Trans.*, 1973, vol. 4, pp. 419–22. <https://doi.org/10.1007/BF02648693>.
10. J. Byerley and W.K. Teo: *J. Inorg. Nucl. Chem.*, 1973, vol. 35(7), pp. 2195–2205. [https://doi.org/10.1016/0022-1902\(73\)80282-9](https://doi.org/10.1016/0022-1902(73)80282-9).
11. I. Tomaszewicz, G.A. Hope, and P.A.G. O'Hare: *J. Chem. Thermodynamics*, 1997, vol. 29(9), pp. 1031–45. <https://doi.org/10.1006/jcht.1997.0221>.
12. M. Skrobjan, N. Sato, M. Saito, and T. Fujino: *J. Alloys Compd.*, 1994, vol. 210(1-2), pp. 291–97. [https://doi.org/10.1016/0925-8388\(94\)90152-x](https://doi.org/10.1016/0925-8388(94)90152-x).
13. M. Skrobjan, N. Sato, and T. Fujino: *Thermochim. Acta*, 1995, vol. 249, pp. 211–19. [https://doi.org/10.1016/0040-6031\(95\)90696-7](https://doi.org/10.1016/0040-6031(95)90696-7).
14. M. Skrobjan, N. Sato, K. Yamada, and T. Fujino: *Thermochim. Acta*, 1995, vol. 255, pp. 201–09. [https://doi.org/10.1016/0040-6031\(94\)02150-M](https://doi.org/10.1016/0040-6031(94)02150-M).
15. M. Saeki, M. Onoda, and Y. Yajima: *J. Sol. State Chem.*, 1996, vol. 121(2), pp. 451–56. <https://doi.org/10.1006/jssc.1996.0062>.
16. S. Hirai, K. Shimakage, Y. Saitou, T. Nishimura, Y. Uemura, M. Mitomo, and L. Brewer: *J. Am. Ceram. Soc.*, 1998, vol. 81(1), pp. 145–51. <https://doi.org/10.1111/j.1151-2916.1998.tb02306.x>.
17. J. Cuya, N. Sato, K. Yamamoto, A. Muramatsu, K. Aoki, and Y. Taga: *Thermochim. Acta*, 2004, vol. 410(1-2), pp. 27–34. [https://doi.org/10.1016/s0040-6031\(03\)00366-6](https://doi.org/10.1016/s0040-6031(03)00366-6).
18. S. Komatsuzaki, K. Takase, C.F. Smura, Y. Takahashi, Y. Takano, K. Sekizawa, and S.J. Clarke: *J. Alloys Compd.*, 2006, vols. 408–412, pp. 586–88. <https://doi.org/10.1016/j.jallcom.2004.12.058>.
19. N. Sato, G. Shinohara, A. Kirishima, and O. Tochiyama: *J. Alloys Compd.*, 2008, vol. 451(1-2), pp. 669–72. <https://doi.org/10.1016/j.jallcom.2007.04.100>.
20. H. Yuan, J. Zhang, R. Yu, and Q. Su: *J. Rare earths*, 2013, vol. 31(3), pp. 327–30. [https://doi.org/10.1016/s1002-0721\(12\)60280-4](https://doi.org/10.1016/s1002-0721(12)60280-4).
21. O.M. Saad, T. Kuzuya, S. Hirai, and M. Ohta: *Mater. Trans.*, 2010, vol. 51(12), pp. 2289–93. <https://doi.org/10.2320/matertrans.m2010157>.
22. M. Ohta, S. Satoh, T. Kuzuya, S. Hirai, M. Kunii, and A. Yamamoto: *Acta Mater.*, 2012, vol. 60, pp. 7232–40. <https://doi.org/10.1016/j.actamat.2012.09.035>.
23. M. Ohta, P. Jood, M. Murata, C-H. Lee, A. Yamamoto, and H. Obara: *Adv. Energy Mater.*, 2019, vol. 9(23), 1801304. <https://doi.org/10.1002/aenm.201801304>.
24. E. Guilmeau, A. Maignan, C. Wan, and K. Koumoto: *Phys. Chem. Chem. Phys.*, 2015, vol. 17, pp. 24541–555. <https://doi.org/10.1039/C5CP01795E>.
25. Y. Kikuchi, Yn. Bouyrie, M. Ohta, K. Suekuni, M. Aihara, and T. Takabatake: *J. Mater. Chem. A*, 2016, vol. 4, pp. 15207–214. <https://doi.org/10.1039/C6TA05945G>.
26. E. Ahmadi, Y. Yashima, R.O. Suzuki, and S.A. Rezan: *Metall. Mater. Trans. B*, 2018, vol. 49(4), pp. 1808–21. <https://doi.org/10.1007/s11663-018-1278-8>.
27. E. Ahmadi and R.O. Suzuki: *Metall. Mater. Trans. B*, 2020, vol. 51(1), pp. 140–48. <https://doi.org/10.1007/s11663-019-01730-w>.
28. N. Suzuki, M. Tanaka, H. Noguchi, S. Natsui, T. Kikuchi, and R.O. Suzuki: *Mater. Trans.*, 2017, vol. 58(3), pp. 367–70. <https://doi.org/10.2320/matertrans.mk201613>.
29. T. Matsuzaki, S. Natsui, T. Kikuchi, and R.O. Suzuki: *Mater. Trans.*, 2017, vol. 58(3), pp. 371–76. <https://doi.org/10.2320/matertrans.m2016305>.
30. T. Kaneko, Y. Yashima, E. Ahmadi, S. Natsui, and R.O. Suzuki: *J. Solid State Chem.*, 2020, vol. 285, p. 121268. <https://doi.org/10.1016/j.jssc.2020.121268>.
31. R.F. Barrow and W. Jevons: *Proc. R. Soc. London A*, 1938, vol. 169(936), pp. 45–65. <https://doi.org/10.1098/rspa.1938.0194>.
32. R. Yokoyama: Japanese patent, S26-3067 filed on 1951.6.13.
33. M. Egashira, H. Katsuki, M. Mori, H. Kaneko, W. Kurahashi, and S. Kawasumi: *Yogyo Kyokai Shi (Bull. Jpn. Ceram. Soc.)*, 1985, vol. 93(9), pp. 535–40. https://doi.org/10.2109/jcersj.1950.93.1081_535.
34. M. Egashira, Y. Ohyama, and H. Katsuki: *J. Ceram. Soc. Jpn.*, 1988, vol. 96(1110), pp. 171–75. <https://doi.org/10.2109/jcersj.96.171>.
35. D.I. Bletskan: *J. Ovonic Research*, 2005, vol. 1(5), pp. 47–52. <http://www.chalcogen.ro/Bletskan.pdf>.
36. A. Roine: *HSC Chemistry, 8.0.8*, Outotec Technologies, Pori, Finland, 2014.
37. *NIST-JANAF thermochemical tables, 4th ed. Part II, Cr-Zr, (Journal of physical and chemical reference data, Monograph: No. 9)*, ed. by Malcolm W. Chase, Jr., National Institute of Standards and Technology, Gaithersburg, MD USA, 1998, p.1867, p.1871 and p.1872.
38. E. Tiede and H. Thimann: *Ber.*, 1926, 59 II B p.1703. Quoted in Ref. 47.
39. E.J. Kohlmeyer and H.W. Retzlaff: *Z. anorg. Chem.*, 1950, vol. 261(3-4), pp. 248–60. <https://doi.org/10.1002/zaac.19502610314>.
40. C. Chen, X. Zhang, L. Krishna, C. Kendrick, S.-L. Shang, E. Toberer, Z.-K. Liu, A. Tamboli, and J.M. Redwing: *J. Crystal Growth*, 2016, vol. 452, pp. 151–57. <https://doi.org/10.1016/j.jcrysgro.2015.12.005>.
41. A. Haas: *Angew. Chem.*, 1965, vol. 77, pp. 1066–75; *Angew. Chem. Int. Ed. Engl.*, 1965, vol. 4(12), pp. 1014–1023. <https://doi.org/10.1002/anie.196510141>.
42. P.A.G. O'Hare: *J. Chem. Thermodyn.*, 1987, vol. 19(7), pp. 675–701. [https://doi.org/10.1016/0021-9614\(87\)90090-5](https://doi.org/10.1016/0021-9614(87)90090-5).
43. M.S. Chandrasekharaiyah and J.L. Margrave: *J. Phys. Chem. Ref. Data*, 1994, vol. 23, pp. 499–507. <https://doi.org/10.1063/1.555960>.

44. J.L. Murray and A.J. McAlister: *Bull. Alloy Phase Diagr.*, 1984, vol. 5, pp. 74–84. <https://doi.org/10.1007/BF02868729>.
45. W.C. Schumb and W.J. Bernard: *J. Am. Chem. Soc.*, 1955, vol. 77(4), pp. 904–05. <https://doi.org/10.1021/ja01609a029>.
46. H.-H. Emons and L. Theisen: *Monat. Chem.*, 1972, vol. 103, pp. 62–71. <https://doi.org/10.1007/BF00912928>.
47. *Handbook of Chemistry and Physics*, 39th ed., Chemical Rubber Publ. Co., 1957–58, p. 598 quoted in Ref. 8.
48. H. Gabriel and C. Alvarez-Tostado: *J. Am. Chem. Soc.*, 1952, vol. 74(1), pp. 262–64. <https://doi.org/10.1021/ja01121a513>.
49. P. Coppens, S. Smoes, and J. Drowart: *Trans. Faraday Soc.*, 1967, vol. 63, pp. 2140–48. <https://doi.org/10.1039/TF9676302140>.
50. R.J. Fruehan and E.T. Turkdogan: *Metall. Trans.*, 1971, vol. 2, pp. 895–902. <https://doi.org/10.1007/BF02662752>.
51. M. Bonnet, J. Rogez, and R. Castanet: *Thermochim. Acta*, 1989, vol. 155, pp. 39–56.
52. H. Yoshida, M. Matsubara, and S. Yoshida: *Kagaku Kougaku Ronbunshu*, 1992, vol. 18(3), pp. 281–87. <https://doi.org/10.1252/kakoronbunshu.18.281>.

Publisher's Note Springer Nature remains neutral with regard to jurisdictional claims in published maps and institutional affiliations.